Chemical Science

ROYAL SOCIETY OF CHEMISTRY

EDGE ARTICLE

View Article Online
View Journal | View Issue

Cite this: *Chem. Sci.*, 2021, **12**, 13434

All publication charges for this article have been paid for by the Royal Society of Chemistry

Role of rare-earth elements in enhancing bioelectrocatalysis for biosensing with NAD^+-dependent glutamate dehydrogenase†

Lihao Guan,[a] Fei Wu,*[b] Guoyuan Ren,[a] Jialu Wang,[a] Xiaoti Yang,[b] Xiaohua Huang,[c] Ping Yu,[b] Yuqing Lin*[a] and Lanqun Mao[bd]

Dehydrogenases (DHs) are widely explored bioelectrocatalysts in the development of enzymatic bioelectronics like biosensors and biofuel cells. However, the relatively low intrinsic reaction rates of DHs which mostly depend on diffusional coenzymes (*e.g.*, NAD^+) have limited their bioelectrocatalytic performance in applications such as biosensors with a high sensitivity. In this study, we find that rare-earth elements (REEs) can enhance the activity of NAD^+-dependent glutamate dehydrogenase (GDH) toward highly sensitive electrochemical biosensing of glutamate *in vivo*. Electrochemical studies show that the sensitivity of the GDH-based glutamate biosensor is remarkably enhanced in the presence of REE cations (*i.e.*, Yb^{3+}, La^{3+} or Eu^{3+}) in solution, of which Yb^{3+} yields the highest sensitivity increase (*ca.* 95%). With the potential effect of REE cations on NAD^+ electrochemistry being ruled out, homogeneous kinetic assays by steady-state and stopped-flow spectroscopy reveal a two-fold enhancement in the intrinsic reaction rate of GDH by introducing Yb^{3+}, mainly through accelerating the rate-determining NADH releasing step during the catalytic cycle. In-depth structural investigations using small angle X-ray scattering and infrared spectroscopy indicate that Yb^{3+} induces the backbone compaction of GDH and subtle β-sheet transitions in the active site, which may reduce the energetic barrier to NADH dissociation from the binding pocket as further suggested by molecular dynamics simulation. This study not only unmasks the mechanism of REE-promoted GDH kinetics but also paves a new way to highly sensitive biosensing of glutamate *in vivo*.

Received 12th January 2021
Accepted 1st September 2021

DOI: 10.1039/d1sc00193k

rsc.li/chemical-science

Introduction

Dehydrogenases (DHs) are essential for catalyzing many oxidative reactions in living biosystems and have been an important part of the bioelectrocatalytic family to be frequently applied in biofuel cells,[1–6] biosensors,[7–12] and biosynthesis.[13–15] The performances of DHs-based bioelectronics involve the enzymatic turnover of substrates with coenzymes and electrochemical regeneration of coenzymes, which are thus determined by the intrinsic enzyme kinetics of DHs and the electron transfer kinetics between enzymes and electrode surface.[16–18] There are a list of strategies to improve the bioelectrocatalytic activity by promoting interfacial electron transfer kinetics, such as tuning the electronic properties of the electrode materials,[12,19,20] selecting appropriate mediators for shuttling electron transfer,[21] engineering nanostructured interfaces or protein structures to regulate enzyme conformation/orientation on the electrode surface.[8,22–25] In addition, chemical regulation of enzyme kinetics is the other efficient means in promoting the complete turnover coupling electrode process, usually by biogenic ions (*e.g.*, Ca^{2+}, Mg^{2+} and Zn^{2+}) or molecules (*e.g.*, ATP).[26] In recent years, rare-earth elements (REEs), non-necessary trace elements for most living organisms on earth, have emerged as new modulators for several enzymes like methanol dehydrogenases,[27–29] and their physiological effects are attracting increasing attention.[30,31]

Glutamate is the primary excitatory neurotransmitter involved in brain functions such as cognition, memory and learning.[32–35] *In vivo* biosensing of glutamate is thus of great significance to understand the physiological role of glutamate. Besides the frequently explored glutamate oxidase,[36] glutamate dehydrogenase (GDH) catalyzing $NAD(P)^+$-dependent glutamate oxidation has received growing interest as the bioelectrocatalytic unit in developing oxygen-insensitive glutamate

[a]*Department of Chemistry, Capital Normal University, Beijing 100048, China. E-mail: linyuqing@cnu.edu.cn*

[b]*Beijing National Laboratory for Molecular Science, Key Laboratory of Analytical Chemistry for Living Biosystems, Institute of Chemistry, University of Chinese Academy of Sciences, Beijing 100049, China. E-mail: wufei317@iccas.ac.cn*

[c]*National and Local Joint Engineering Research Center of Biomedical Functional Materials, Jiangsu Collaborative Innovation Center of Biomedical Functional Materials, School of Chemistry and Materials Science, Nanjing Normal University, Nanjing 210023, China*

[d]*College of Chemistry, Beijing Normal University, Beijing 100875, China*

† Electronic supplementary information (ESI) available. See DOI: 10.1039/d1sc00193k

biosensors. Being a hexamer of identical 501-residue polypeptide chains, GDH contains two functional domains respectively for glutamate binding and NAD^+ binding, with a flexible "antenna" coupling the distinct domains through a conformational switch during catalytic turnover (Fig. 1).[37–39] The two-substrate enzymatic reaction undergoes an ordered bi–bi scheme,[40] so the bioelectrocatalytic performance is not only determined by glutamate dynamics but also heavily dependent on NAD^+ association and NADH dissociation. In this regard, ions and molecules that have an effect on the enzyme conformation or binding dynamics at the active site are potential modulators of GDH-based biosensors. A number of biogenic GDH activators and inhibitors have indeed been reported,[38] but are unexplored in an electrochemical scheme. Gao *et al.* made the pioneering discovery that REEs in trivalent forms can regulate the bioelectrocatalytic activity of GDH[41,42] through a "hormesis effect", *i.e.*, REEs at low concentrations can activate GDH, while inhibit GDH at high concentrations.[29,43] This finding implies that REEs in low quantities may be efficient enzyme promoters to improve the sensitivity of GDH-based glutamate biosensors, while the underlying mechanism needs further clarification.

Here, we report an investigation of the role of trivalent REEs (*i.e.*, Yb^{3+}, La^{3+} and Eu^{3+}) in promoting electrochemical oxidation of glutamate catalysed by NAD^+-dependent GDH. The presence of REEs at low micromolar levels in the electrolyte amplified current responses of the GDH-based biosensor to glutamate titrations by maximally 100%, mainly through accelerating the rate-determining NADH release. Protein conformational analysis and molecular dynamics (MD) simulation revealed that REE coordination to GDH can induce partial backbone reconfiguration into a more compact state and may assist NADH dissociation. Our efforts provide an allosteric mechanism for REE-enhanced GDH kinetics and bioelectrocatalysis, and bring up a new class of promoters for constructing highly sensitive glutamate biosensors for *in vivo* analysis.

Results and discussion

Role of REEs in bioelectrocatalysis of NAD^+-dependent GDH

The overall bioelectrocatalytic cycle of NAD^+-dependent GDH can be divided into two processes, the chemical process where GDH catalyzes oxidative deamination of glutamate to α-ketoglutarate while reducing NAD^+ to NADH, and the electrode process where NADH is electro-oxidized back to NAD^+ for the subsequent cycle. In order to probe the role of REEs during the cycle, we first performed electrochemical characterizations to unravel the impact of REEs on the bioelectrocatalytic performance of NAD^+-dependent GDH. The GDH-based electrochemical glutamate biosensors were designed with glassy carbon electrodes (GCEs) modified by adsorbed GDH and methylene green (MG), the electrocatalyst for NADH oxidation at 0.0 V (*vs.* Ag/AgCl) to regenerate NAD^+, and tested by amperometric titrations in artificial cerebrospinal fluid (aCSF, pH 8.5) containing NAD^+ in the absence or presence of Yb^{3+}, La^{3+} or Eu^{3+}. As shown in Fig. 2a, the oxidation current of the GDH-based biosensor increases upon glutamate titrations, demonstrating the successful build-up of the electrode-coupled glutamate oxidation catalytic cycle. In REE-free aCSF the glutamate sensing sensitivity is 16.6 nA μM^{-1} cm^{-2}. While in the presence of Yb^{3+}, La^{3+} or Eu^{3+}, the sensitivity increases by 94.6% (32.3 nA μM^{-1} cm^{-2}), 88.6% (31.3 nA μM^{-1} cm^{-2}) or 16.9% (19.4 nA μM^{-1} cm^{-2}), respectively (Fig. 2b).

As the current response is not only an outcome of GDH catalysis but also of NAD^+ regeneration on the electrode, it is necessary to clarify whether REEs promote the electrochemical oxidation of NADH. We compared cyclic voltammograms of NADH oxidation before and after the introduction of Yb^{3+}. As depicted in Fig. S2a,† the oxidation of MG occurred at −0.10 V at the MG-modified GCE and the oxidation peak current was remarkably enhanced with the addition of 1 mM NADH, which was ascribed to the electrocatalytic oxidation of NADH by MG. After Yb^{3+} was introduced into the solution, the oxidation peak current remained almost the same as that without Yb^{3+}. In addition, the effect of Yb^{3+} on the electrocatalytic NADH

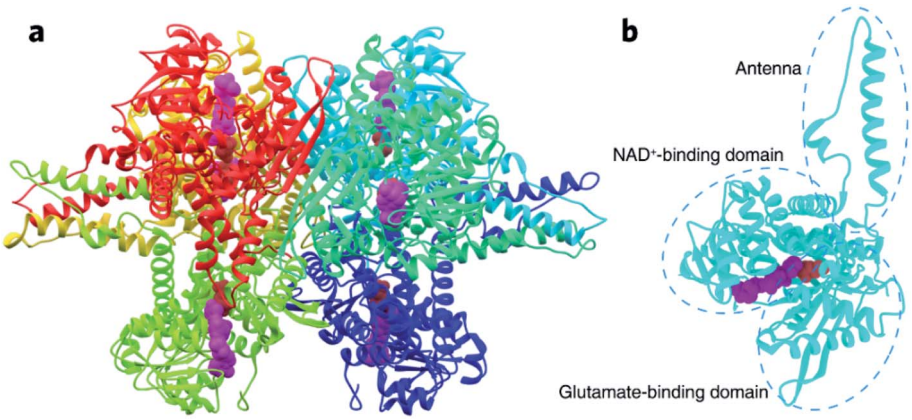

Fig. 1 Crystal structure of GDH from bovine liver (PDB: 1HWY). (a) The entire hexamer of GDH with bound NAD^+ (represented by purple spheres) and glutamate (represented by red spheres). (b) GDH subunit consisting of the NAD^+-binding domain, glutamate-binding domain, and connecting antenna.

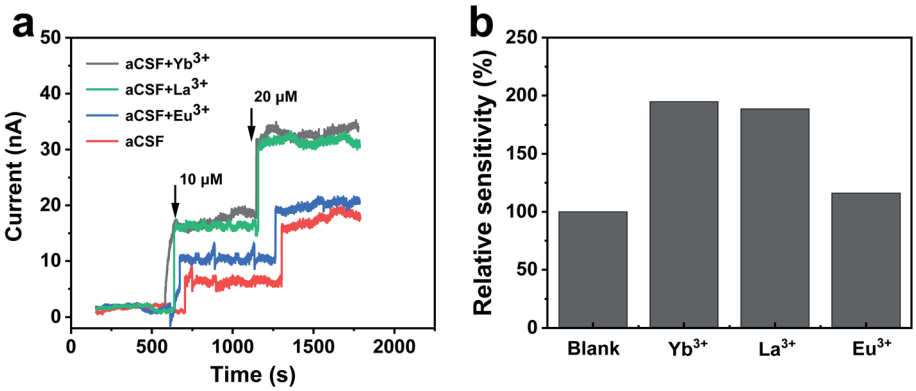

Fig. 2 Effect of REEs on bioelectrocatalytic performance of NAD^+-dependent GDH. (a) Amperometric current responses of the GDH-based biosensor toward titrations of 10 and 20 μM glutamate at 0.0 V *vs.* Ag/AgCl in aCSF containing 2 mM NAD^+ in the absence or presence of 16 μM Yb^{3+}, La^{3+} or Eu^{3+}. (b) Relative sensitivity of the GDH-based glutamate biosensor.

oxidation was evaluated by chronoamperometry. The addition of Yb^{3+} into aCSF containing NADH did not produce a recordable current response, as displayed in Fig. S2b,† revealing that REEs do not enhance the electrochemical oxidation of NADH. Consequently, it can be deduced that Yb^{3+} probably promotes the bioelectrocatalysis of GDH for glutamate sensing through the catalytic turnover within GDH.

After ruling out the involvement of REEs in the electrode process, we proposed that REEs may exert a promotive effect on enzymes in the chemical process. We thus conducted steady-state activity assays in a homogeneous setup to confirm our speculation. NADH production was monitored at 340 nm by UV-vis spectroscopy in a mixture of GDH, NAD^+ and glutamate with or without Yb^{3+}. As displayed in Fig. 3a, the absorbance profiles over time show a faster generation of NADH with GDH in aCSF containing Yb^{3+} after reactions reach the steady state (5 s after mixing). We collected data points within the beginning 10–30 s of the profiles to evaluate enzyme activity in terms of initial reaction rate. From the slope of linear fitting plots, we obtained the overall turnover rate of GDH to be 1.24 ± 0.0037 μM s^{-1} in the presence of 16 μM Yb^{3+}, approximately 195% increase from 0.42 ± 0.0067 μM s^{-1} in blank aCSF (Fig. 3b, $n = 3$). As the concentration of Yb^{3+} doubled (32 μM), the increase in the turnover rate became smaller (1.51 times, Fig. S3†), indicating the concentration dependence of the Yb^{3+}-induced enhancement, which can be explained by the hormesis effect.[41,43,44]

Mechanism for REE-promoted NAD^+-dependent GDH catalysis

The complete catalytic cycle of GDH is a sequence of four kinetic phases involving proton release, hydride transfer, intermediary complex transformation and product release as previously reported.[40,45–47] Transient-state kinetic assays by stopped-flow spectroscopic measurements herein also resolved four distinguishable phases (Fig. 4a). Within 3 ms upon mixing of GDH–NAD^+ and glutamate (Glu) solutions, a complex of GDH–NAD^+–Glu forms as the starting point to trigger the sequential reaction

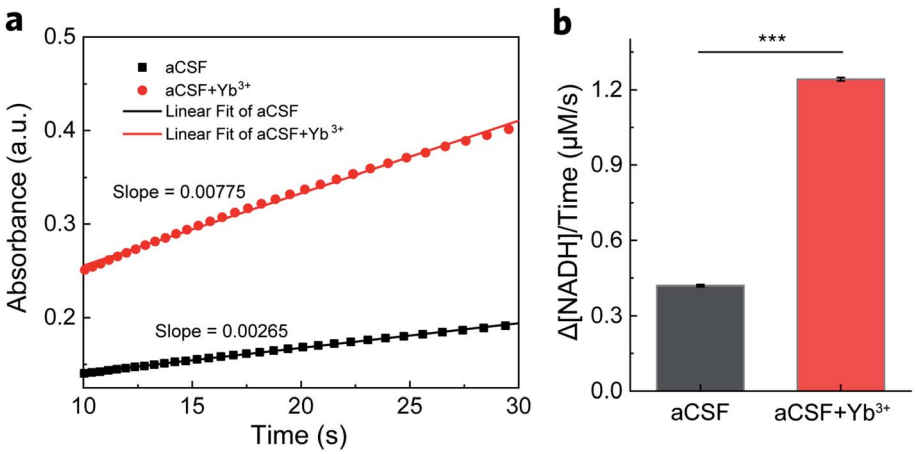

Fig. 3 Steady-state GDH activity assay. (a) The absorbance of NADH at 340 nm generated in aCSF containing 0.1 mg mL^{-1} (*ca.* 300 nM) GDH, 250 μM NAD^+ and 5 mM glutamate in the absence and presence of 16 μM Yb^{3+}. Linear fitting of the steady-state profile during 10–30 s yields the corresponding slope for reaction rate calculation. (b) The calculated overall reaction rate of NADH production in the absence and presence of 16 μM Yb^{3+}. Error bars represent standard error of the mean ($n = 3$, *t*-test, ***$P < 0.001$).

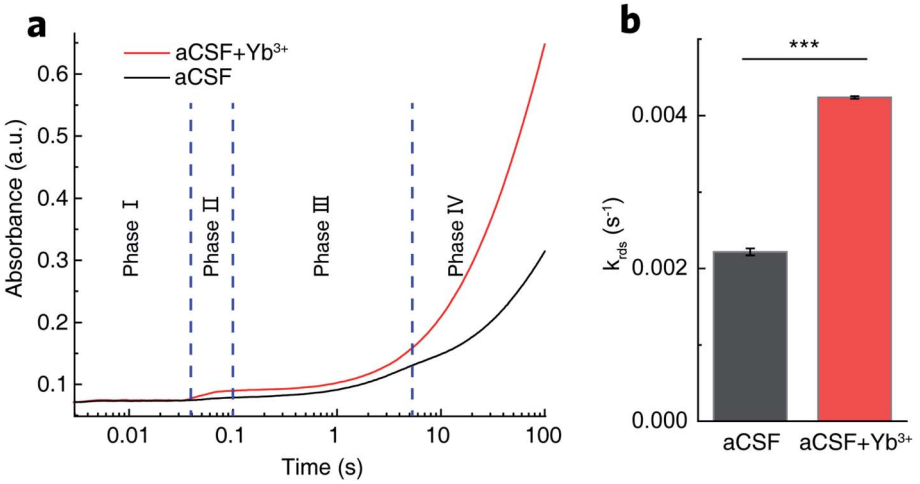

Fig. 4 Transient-state GDH kinetics. (a) Typical absorbance profiles at 340 nm over 100 s showing four distinguishable phases of GDH-catalyzed glutamate oxidation in aCSF containing 0.1 mg mL^{-1} GDH, 250 μM NAD^+ and 5 mM glutamate in the absence (black) and presence (red) of 16 μM Yb^{3+} by stopped-flow spectroscopy. (b) Rate constants of the rate-determining NADH release in phase IV obtained by fitting the absorbance profile during 10–1500 s using two consecutive one-order kinetic modeling. Error bars represent standard error of the mean ($n = 3$, t-test, ***$P <$ 0.001).

process. Phase I (3–30 ms) illustrates the proton release step prior to hydride transfer. Then in phase II (30–100 ms), hydride transfer bursts between bound glutamate and NAD^+ to result in the ternary complex of GDH, NADH and α-iminoglutarate, the latter accepting one molecule of H_2O from Lys. 126 accompanied by a conformational change of GDH to form α-carbinolamine that subsequently deaminates into α-ketoglutarate.[37,45,48] In phase III (100 ms to 4 s), glutamate slowly displaces α-ketoglutarate in the binding pocket.[45,49] The final phase IV is the steady-state release of NADH that takes the longest period of time, and thus is the rate-determining step (RDS).[50]

By fitting the curves of phase IV into a kinetic model of two continuous one-order reactions, we acquired the apparent rate constant (k_{rds}) to be (2.22 ± 0.05) × 10^{-3} s^{-1} in REE-free aCSF. With Yb^{3+} present, k_{rds} was determined to be (4.24 ± 0.02) × 10^{-3} s^{-1} (Fig. 4b). The kinetic enhancement on phase IV (91%) demonstrates that Yb^{3+} does promote NADH release. Moreover, we measured the respective rate constants for phase I (k_1), II (k_2) and III (k_3), summarized in Table S1.† No statistical kinetic difference was observed during phase I, but k_2 and k_3 increased respectively by 51% and 40% in Yb^{3+}-containing aCSF, implying that Yb^{3+} might also facilitate hydride transfer, intermediary complex transformation and displacement of α-ketoglutarate by glutamate.

To uncover the structural basis for the promotive effects of Yb^{3+} indicated by the transient-state kinetic study above, we first employed small angle X-ray scattering (SAXS) to probe possible Yb^{3+}-induced conformational alterations in solvated GDH. The scattering intensity, $I(q)$, measured from isotropically monodispersed GDH ligand with NAD^+ in aCSF demonstrated its globular form in dilute solution (Fig. 5a). Modeling the indirect inverse Fourier transform of $I(q)$ produced the real-space distribution profile, $p(r)$, which describes pair distances between scattering centers of enzyme molecules (Fig. 5b).[51,52] The radius of gyration (R_g) yielding size information for polymeric molecules was then extracted from $p(r)$,[53] and determined as 6.39 ± 0.19 nm for GDH in blank aCSF. After introducing Yb^{3+}, GDH exhibited a smaller R_g of 5.66 ± 0.16 nm (Fig. 5c). Reduction in protein size excluded the probability of REE-induced enzyme aggregation while reflected higher compactness of the GDH entity, in accordance with the reported conformational modulation of proteins by REEs, such as the structural compaction in the cases of calmodulin and lanmodulin.[39,54] Based on this result, we hypothesized that Yb^{3+} cations might coordinate electron-sufficient moieties at the active site and bring domains or local residues in closer proximity (Fig. 5d). In consequence they may reduce the spatial gap for hydride transfer and/or nucleophilic attack on α-iminoglutarate by Lys. 126-bonded H_2O to form α-ketoglutarate,[55] explaining the increase of k_2 in phase II.

To confirm our hypothesis of Yb^{3+} localization in GDH, we conducted attenuated total reflectance-Fourier transform infrared (ATR-FTIR) spectroscopic investigations to probe regional transitions triggered by inner-bound Yb^{3+}. The amide I band between 1700 and 1600 cm^{-1}, originating from the stretching vibration of C=O bonds in protein backbones and highly sensitive to secondary structural changes,[19,56–58] was selected from the full IR spectra of GDH for further deconvolution (Fig. 6a). We used fourth derivation to identify peak positions of convoluted bands related to different secondary structures (Fig. 6b). Notably, Yb^{3+} exerted no effect on band positions except that the vibrational peak of flexible β-sheets centered in the high-frequency vibrational range (HF-β-sheets, 1697 cm^{-1}) was slightly shifted to 1692 cm^{-1} in Yb^{3+}-treated GDH. Lower vibrational frequency indicated the loss in backbone flexibility of β-sheets that were loosely packed. This phenomenon is in line with SAXS observation of gain in backbone tightness upon Yb^{3+} coordination. We then resolved the

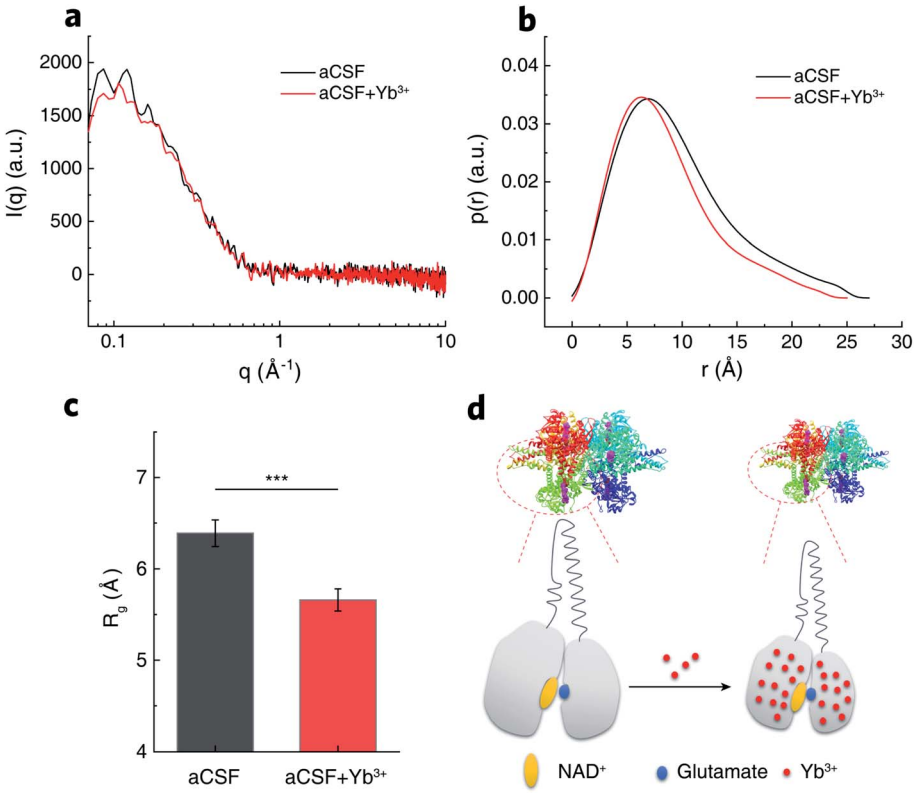

Fig. 5 Protein conformation of GDH. (a) Scattering intensities of GDH in aCSF containing NAD^+ in the absence (black) and presence (red) of Yb^{3+} by SAXS. (b) Corresponding pair distances distribution function obtained from (a). (c) R_g encoding protein size information calculated from (b). Error bars represent standard error of the mean ($n = 8$, t-test, ***$P < 0.001$). (d) Schematic illustration of Yb^{3+}-induced GDH conformation change into a more compact state.

secondary component bands by Gaussian fitting for proportion calculation (Fig. S4†). As shown in Fig. 6c, α-helices and β-sheets prevailed in solvated GDH with a minor distribution of turns and the unordered. Compared to the secondary composition in blank aCSF, α-helices were almost unaffected by Yb^{3+}, but the proportion of β-sheets decreased by 6.7%. In the meantime, the proportion of β-turns increased by 9%. According to the crystal structure of GDH,[35] α-helices establish the main protein scaffold, while β-sheets gather at the glutamate and NAD^+-binding sites (Fig. 6d). In this regard, IR results indicated the possible localization of Yb^{3+} in the active site that caused a subtle transition from β-sheets to β-turns. This may lead to a plausible configuration of one Yb^{3+} ion coordinated to Glu. 275, Ser. 276 and Asp. 277 consecutively in a β-turn in the vicinity of bound NAD^+/NADH (Fig. 6e).

As shown in stopped-flow measurements, major kinetic promotion stemmed from phase IV acceleration (91%) by Yb^{3+}. Meanwhile, SAXS and IR characterizations suggest the possible localization of Yb^{3+} at the active site. Taken together, we proposed two models of the Yb^{3+} coordination configuration by MD simulations. Because REEs prefer an octadentate coordination,[30] one hydrated Yb^{3+} ion is ligated to seven water molecules and the carboxylic side chain of Asp. 277 in one model (Fig. S5a†). Glu. 275 forms a hydrogen bond with one water ligand of Yb^{3+}. In the other model (Fig. S5b†), both Asp. 277 and Glu. 275 are in the primary coordination sphere of Yb^{3+} with the rest occupied by six water molecules. Existence of these two types of configurations suggests the dynamic feature of Yb^{3+} coordination influenced by electrostatic forces and hydrogen bonding. Ser. 276 was not found involved in anchoring Yb^{3+} in either situation. Computed free energy over the distance describes a four-stage course of NADH dissociation from the center of the binding pocket (Fig. S5c and S6†). In the initial stage, NADH within 0.5 nm away from the binding sites (still inside the pocket) experiences comparable free energies (around 120 kJ mol^{-1}). As NADH continues leaving the binding sites, electrostatic attractive force from Asp. 277 and/or Glu. 275 retards its leaving in terms of increased free energy. Yb^{3+} coordination to these negatively charged residues weakens the electrostatic attraction between the amine moiety of NADH and the side carboxylates of residues. The total free energy for NADH release was 381 kJ mol^{-1} and 303 kJ mol^{-1} in the absence and presence of Yb^{3+}, respectively. This remarkable energetic reduction in the kinetic barrier (*ca.* 80 kJ mol^{-1}) for the RDS may be the primary factor that promotes GDH catalysis.

Implication for sensitive glutamate biosensing *in vivo*

Knowing that REEs can efficiently enhance the bioelectrocatalytic activity of NAD^+-dependent GDH, we were in a position to explore the applicability of REEs in promoting

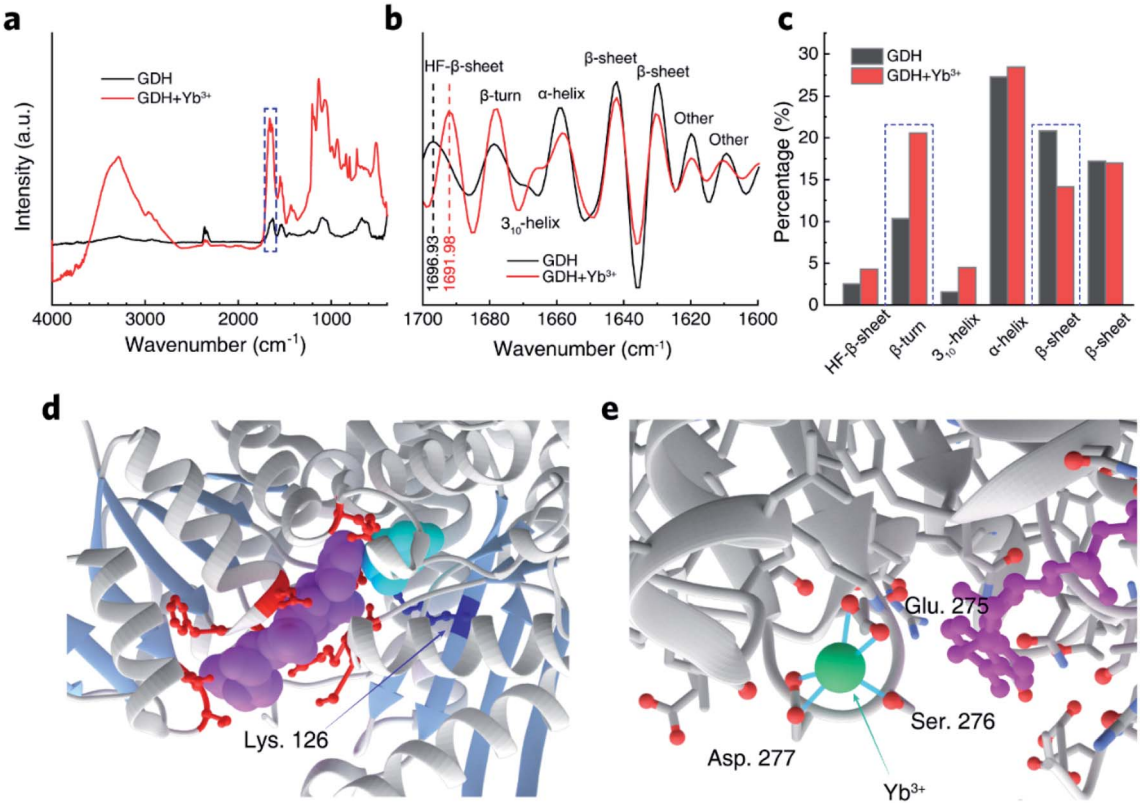

Fig. 6 Regional changes of GDH structure. (a) ATR-FTIR spectra of GDH pre-incubated with or without Yb^{3+}. Dashed frame denotes the amide I band region. (b) Fourth derivation of amide I band. (c) Compositional percentages of different GDH secondary structures by integrating peak areas of deconvoluted bands. (d) Zoomed image of GDH active site with bound NADH (purple), glutamate (cyan) and residues binding NADH (red). Lys. 126 attacking glutamate intermediate and β-sheets guarding the active site are highlighted in dark blue and light blue, respectively. (e) The most plausible anchoring site for Yb^{3+} facing three potential ligand residues, Glu. 275, Ser. 276 and Asp. 277, which constitute a β-turn near bound NADH.

biosensing sensitivity *in vivo*. To do this, an online electrochemical analytical system (OECS) was constructed for continuous monitoring of glutamate as illustrated in Fig. S7a.† Two streams of aCSF solutions with different compositions (one for brain dialysate collection and the other for NAD^+ and Yb^{3+} supply) were continuously perfused by microinjection pumps and loaded into an electrochemical flow cell equipped with GDH-MG-modified GCE as the glutamate probe. Fig. S7b† compares the online glutamate sensing results in the presence and absence of Yb^{3+}, showing that Yb^{3+} dramatically enhanced the online current responses. The OECS displayed a good linear response with glutamate concentration ranging from 4 to 100 μM (I (nA) = $1.01C_{\text{glutamate}}$ (μM) + 11.36, $R^2 = 0.98$) (Fig. S7c†). The detection limit, based on a signal-to-noise ratio of 3, was calculated to be 2.92 ± 0.11 μM. During online brain analysis, a large current increase was recorded for the brain microdialysate continuously sampled from the striatum of rats (Fig. S7d†), validating the applicability of the Yb^{3+}-promoted, GDH-based OECS for *in vivo* real-time biosensing of glutamate. The basal dialysate level of glutamate in the rat striatum was determined to be 4.52 ± 0.27 μM ($n = 3$), consistent with the reported basal range of glutamate in extracellular space (4 to 350 μM).[59–62] Taken together, the OECS equipped with REEs and GDH could be used as an effective and sensitive platform to record the basal level and dynamics of glutamate under physiological and pathological conditions *in vivo*.

Conclusions

In summary, by investigating the interaction mechanism between Yb^{3+} and GDH, we have successfully demonstrated that REEs serve as allosteric promoters for bioelectrocatalysis of GDH by triggering subtle reorientation of peptide segments, consequently expediting phase coupling along with the catalytic scheme. Steady-state and transient-state spectroscopic investigations clarified the role of Yb^{3+} in modulating GDH kinetics and showed that Yb^{3+} in low quantity introduces a two-fold increase of the entire turnover rate by promoting the glutamate intermediate conversion to α-ketoglutarate and releasing of reduced coenzyme (*i.e.*, NADH). Furthermore, the molecular basis of Yb^{3+} as the GDH promoter was unmasked by conformational analysis, *i.e.*, SAXS and ATR-FTIR spectroscopy, and the results indicated that binding of Yb^{3+} with GDH leads to a narrower enzyme body accompanied by transitions of β-sheets to β-turns at the active site. In consequence, the total free energy for NADH release in the rate-determining step was reduced by

about 80 kJ mol^{-1} as suggested by MD simulation. This mechanism lays the foundation for the development of new REEs-based regulatory tools for GDH-based biosensors, especially for regulating and monitoring glutamate levels *in vivo* toward neuromodulation and neurodegenerative diseases treatment. Furthermore, this research will shed light on a broad investigation of enzymes in the bioelectrochemistry area from a unique perspective into interactions between REEs and non-metallic NAD^+-dependent DHs.

Data availability

All the data have been included in the ESI.†

Author contributions

L. M., Y. L. and F. W. conceived the idea for the project. L. G. purified the enzyme and conducted the experiments of stopped-flow, SAXS and ATR-FTIR measurements. G. R. and J. W. performed the electrochemical experiments. L. G., F. W. and Y. L. studied the reaction mechanism, analyzed enzyme conformation changes and designed MD simulation. L. G., F. W. and Y. L. drafted the manuscript. L. M., X. Y., P. Y. and X. H. finalized the manuscript. All authors discussed and commented on the manuscript.

Conflicts of interest

There are no conflicts of interest to declare.

Acknowledgements

This work was supported by the National Key Research and Development Program (Grant No. 2018YFE0200800), the National Natural Science Foundation of China (No. 22074095 for Y. Lin; No. 21790390, 21790391 and 22134002 for L. Mao; No. 21874139 and 21927804 for F. Wu), the National Basic Research Program of China (2016YFA0200104), the Strategic Priority Research Program of Chinese Academy of Sciences (XDB30000000), Chinese Academy of Sciences (QYZDJ-SSW-SLH030), and High-level Teachers in Beijing Municipal Universities in the Period of 13th Five year Plan (CIT&TCD20190330). We are grateful to Prof. T. S. Shi (Hebei University) for help with stopped-flow experiments.

Notes and references

1 J. A. Cracknell, K. A. Vincent and F. A. Armstrong, *Chem. Rev.*, 2008, **108**, 2439–2461.
2 L. Xia, K. Van Nguyen, Y. Holade, H. Han, K. Dooley, P. Atanassov, S. Banta and S. D. Minteer, *ACS Energy Lett.*, 2017, **2**, 1435–1438.
3 Y. Ulyanova, M. A. Arugula, M. Rasmussen, E. Pinchon, U. Lindstrom, S. Singhal and S. D. Minteer, *ACS Catal.*, 2014, **4**, 4289–4294.
4 Y. H. Kim, E. Campbell, J. Yu, S. D. Minteer and S. Banta, *Angew. Chem., Int. Ed.*, 2013, **52**, 1437–1440.
5 C. Ji, J. Hou, K. Wang, Y. H. Ng and V. Chen, *Angew. Chem., Int. Ed.*, 2017, **56**, 9762–9766.
6 M. T. Meredith and S. D. Minteer, *Annu. Rev. Anal. Chem.*, 2012, **5**, 157–179.
7 S. Guo, P. Yu, W. Li, Y. Yi, F. Wu and L. Mao, *J. Am. Chem. Soc.*, 2020, **142**, 2074–2082.
8 Z. Guo, L. Murphy, V. Stein, W. A. Johnston, S. Alcala-Perez and K. Alexandrov, *J. Am. Chem. Soc.*, 2016, **138**, 10108–10111.
9 S. Velasco-Lozano, M. Roca, A. Leal-Duaso, J. A. Mayoral, E. Pires, V. Moliner and F. López-Gallego, *Chem. Sci.*, 2020, **11**, 12009–12020.
10 L. Zhang, M. Zhou and S. Dong, *Anal. Chem.*, 2012, **84**, 10345–10349.
11 S. Tsujimura, K. Murata and W. Akatsuka, *J. Am. Chem. Soc.*, 2014, **136**, 14432–14437.
12 G. Wu, Y. Gao, D. Zhao, P. Ling and F. Gao, *ACS Appl. Mater. Interfaces*, 2017, **9**, 40978–40986.
13 J. Kreuzer, N. C. Bach, D. Forler and S. A. Sieber, *Chem. Sci.*, 2015, **6**, 237–245.
14 F. Dong, H. Chen, C. A. Malapit, M. B. Prater, M. Li, M. Yuan, K. Lim and S. D. Minteer, *J. Am. Chem. Soc.*, 2020, **142**, 8374–8382.
15 S. V. Lozano, M. Roca, A. L. Duaso, J. A. Mayoral, E. Pires, V. Moliner and F. L. Gallego, *Chem. Sci.*, 2020, **11**, 12009–12020.
16 P. Das, M. Das, S. R. Chinnadayyala, I. M. Singha and P. Goswami, *Biosens. Bioelectron.*, 2016, **79**, 386–397.
17 A. J. Gross, X. Chen, F. Giroud, C. Travelet, R. Borsali and S. Cosnier, *J. Am. Chem. Soc.*, 2017, **139**, 16076–16079.
18 I. S. Kucherenko, O. O. Soldatkin, D. Y. Kucherenko, O. V. Soldatkina and S. V. Dzyadevych, *Nanoscale Adv.*, 2019, **1**, 4560–4577.
19 F. Wu, L. Su, P. Yu and L. Mao, *J. Am. Chem. Soc.*, 2017, **139**, 1565–1574.
20 M. T. D. Martino, F. Tonin, N. A. Yewdall, M. Abdelghani, D. S. Williams, U. Hanefeld, F. P. J. T. Rutjes, L. K. E. A. Abdelmohsen and J. C. M. van Hest, *Chem. Sci.*, 2020, **11**, 2765–2769.
21 F. Wu, P. Yu, X. Yang, Z. Han, M. Wang and L. Mao, *J. Am. Chem. Soc.*, 2018, **140**, 12700–12704.
22 Y. Xiao, F. Patolsky, E. Katz, J. F. Hainfeld and I. Willner, *Science*, 2003, **299**, 1877–1881.
23 Y. Zhang, Y. Deng, C. Wang, L. Li, L. Xu, Y. Yu and X. Su, *Chem. Sci.*, 2019, **10**, 5959–5966.
24 J. F. Darby, M. Atobe, J. D. Firth, P. Bond, G. J. Davies, P. O'Brien and R. E. Hubbard, *Chem. Sci.*, 2017, **8**, 7772–7779.
25 Y. B. Shpigler and D. Avnir, *Chem. Sci.*, 2020, **11**, 3965–3977.
26 R. C. Hudson, L. D. Ruttersmith and R. M. Daniel, *Biochim. Biophys. Acta*, 1993, **1202**, 244–250.
27 A. Pol, T. R. M. Barends, A. Dietl, A. F. Khadem, J. Eygensteyn, M. S. M. Jetten and H. J. M. Op den Camp, *Environ. Microbiol.*, 2014, **16**, 255–264.
28 Y. W. Deng, S. Y. Ro and A. C. Rosenzweig, *J. Biol. Inorg Chem.*, 2018, **23**, 1037–1047.

29 A. McSkimming, T. Cheisson, P. J. Carroll and E. J. Schelter, *J. Am. Chem. Soc.*, 2018, **140**, 1223–1226.
30 T. Cheisson and E. J. Schelter, *Science*, 2019, **363**, 489–493.
31 J. A. Cotruvo, E. R. Featherston, J. A. Mattocks, J. V. Ho and T. N. Laremore, *J. Am. Chem. Soc.*, 2018, **140**, 15056–15061.
32 D. J. Rossi, T. Oshima and D. Attwell, *Nature*, 2000, **403**, 316–321.
33 I. Ahmed, S. K. Bose, N. Pavese, A. Ramlackhansingh, F. Turkheimer, G. Hotton, A. Hammers and D. J. Brooks, *Brain*, 2011, **134**, 979–986.
34 S. C. Buckingham, S. L. Campbell, B. R. Haas, V. Montana, S. Robel, T. Ogunrinu and H. Sontheimer, *Nat. Med.*, 2011, **17**, 1269–1274.
35 K. Takikawa, D. Asanuma, S. Namiki, H. Sakamoto, T. Ariyoshi, N. Kimpara and K. Hirose, *Angew. Chem., Int. Ed.*, 2014, **53**, 13439–13443.
36 R. D. O'Neill, S.-C. Chang, J. P. Lowry and C. J. McNeil, *Biosens. Bioelectron.*, 2004, **19**, 1521–1528.
37 T. J. Smith, P. E. Peterson, T. Schmidt, J. Fang and C. A. Stanley, *J. Mol. Biol.*, 2001, **307**, 707–720.
38 T. J. Smith and C. A. Stanley, *Trends Biochem. Sci.*, 2008, **33**, 557–564.
39 P. E. Peterson and T. J. Smith, *Structure*, 1999, **7**, 769–782.
40 R. C. Hudson and R. M. Daniel, *Comp. Biochem. Physiol. B-Biochem. Mol. Biol.*, 1993, **106**, 767–792.
41 W. K. Xin and X. X. Gao, *Analyst*, 1996, **121**, 687–690.
42 Q.-K. Zhuang, H.-C. Dai, X.-X. Gao and W.-K. Xin, *Bioelectrochemistry*, 2000, **52**, 37–41.
43 E. Agathokleous, M. Kitao and E. J. Calabrese, *Environ. Pollut.*, 2018, **238**, 1044–1047.
44 L. Wang, A. Lu, T. Lu, X. Ding and X. Huang, *Biochimie*, 2010, **92**, 41–50.
45 N. Singh, S. J. Maniscalco and H. F. Fisher, *J. Biol. Chem.*, 1993, **268**, 21–28.
46 H. F. Fisher, S. Maniscalco, N. Singh, R. N. Mehrotra and R. Srinivasan, *Biochim. Biophys. Acta, Proteins Proteomics*, 1992, **1119**, 52–56.
47 E. Silverstein and G. Sulebele, *Biochemistry*, 1973, **12**, 2164–2172.
48 M. Iwatsubo and D. Pantaloni, *Bull. Soc. Chem. Biol.*, 1967, **49**, 1563.
49 A. Colen, R. Wilkinson and H. Fisher, *J. Biol. Chem.*, 1975, **250**, 5243–5246.
50 H. F. Fisher, *Methods Enzymol.*, Elsevier, 1985, vol. 113, pp. 16–27.
51 C. M. Jeffries, M. A. Graewert, C. E. Blanchet, D. B. Langley, A. E. Whitten and D. I. Svergun, *Nat. Protoc.*, 2016, **11**, 2122–2153.
52 G. L. Hura, A. L. Menon, M. Hammel, R. P. Rambo, F. L. Poole, Ii, S. E. Tsutakawa, F. E. Jenney, Jr, S. Classen, K. A. Frankel and R. C. Hopkins, *Nat. Methods*, 2009, **6**, 606–612.
53 L. Pollack, M. W. Tate, A. C. Finnefrock, C. Kalidas, S. Trotter, N. C. Darnton, L. Lurio, R. H. Austin, C. A. Batt, S. M. Gruner and S. G. J. Mochrie, *Phys. Rev. Lett.*, 2001, **86**, 4962–4965.
54 J. A. Mattocks, J. V. Ho and J. A. Cotruvo, *J. Am. Chem. Soc.*, 2019, **141**, 2857–2861.
55 J. E. Rife and W. W. Cleland, *Biochemistry*, 1980, **19**, 2328–2333.
56 S. Krimm and J. Bandekar, *Adv. Protein Chem.*, 1986, **38**, 181–364.
57 J. Bandekar, *Biochim. Biophys. Acta, Proteins Proteomics*, 1992, **1120**, 123–143.
58 H. Yang, S. Yang, J. Kong, A. Dong and S. Yu, *Nat. Protoc.*, 2015, **10**, 382–396.
59 S. Chakraborty and C. Retna Raj, *Electrochem. Commun.*, 2007, **9**, 1323–1330.
60 A. M. Andrews, A. Schepartz, J. V. Sweedler and P. S. Weiss, *J. Am. Chem. Soc.*, 2014, **136**, 1–2.
61 Y. Yu, X. Liu, D. Jiang, Q. Sun, T. Zhou, M. Zhu, L. Jin and G. Shi, *Biosens. Bioelectron.*, 2011, **26**, 3227–3232.
62 C.-S. Yang, P.-J. Tsai, N.-N. Lin, L. Liu and J.-S. Kuo, *Free Radical Biol. Med.*, 1995, **19**, 453–459.